Molecular structure of Se-rich amorphous films

V. I. MIKLA[*], V. V. MIKLA

Institute for Solid State Physics and Chemistry, Uzhgorod National University, Uzhgorod, Voloshina St. 54, Ukraine

Structure and its transformation are examined for amorphous Se-rich As_xSe_{1-x} ($0 \leq x \leq 0.2$) alloys by employment of diffraction and non-diffraction structural probes. It is shown that the molecular structure of amorphous Se (a-Se) on the scale of short-range order is close to that of crystalline phase, while medium-range order differs from the structure of most inorganic glasses and may be placed between three-dimensional network glasses and polymeric ones. Further experiments show the existence of successive phases in laser-induced glass-crystalline transition with pronounced threshold behavior. Below the energy density threshold, E_{th}, only small changes in the local structure of the system can be detected. Above E_{th}, the changes were attributed to crystallization transformation. The corresponding Raman spectra reveal transformation of the system from amorphous into the crystalline phase under laser irradiation. In the binary As_xSe_{1-x} glass system, a change of structural regime takes place near the composition $x \approx 0.04$. The presence of this topological threshold is established by direct and indirect evidence, such as peculiarities in the composition dependence of the basic parameters for electron diffraction and Raman vibrational modes. The peculiarities are caused by the transition from a chain-ring-like structure to chain-like structure.

1. Introduction

Amorphous selenium has been extensively studied over the past 70 years, but its molecular structure is still disputable. For a long time it was believed that the amorphous phase consisted of selenium chain, Se_n, and 8-ring, Se_8, structures mixed together. This model arose from the fact that in the crystalline phase, selenium can exist in two forms, α-monoclinic Se (α-Se) and trigonal Se (γ-Se). The former consisted of Se_8 rings and the latter of Se_n chains. Reasonably, one can consider a structure for the amorphous phase based on a mixture of ring and chain members. However, the length of the selenium chains is uncertain. In addition, it is unclear whether a-Se contains cyclic structure or rings.

In recent years there has been enhanced interest in structural studies of chalcogenide glasses owing to their imaging applications. As-containing chalcogenides, especially Se-rich alloys, usually have been studied in thin film form. Since change in the structure can have an influence on photogeneration, charge carriers transport, trapping and other important fundamental properties, knowledge of the molecular structure of such materials is needed for further improvement of their characteristics [1-11].

Undoubtedly, elemental semiconductors are useful and suitable testing objects for studying the influence of structure on physical properties [5-7, 12-19]. This is particularly true in respect of selenium. In the past, the latter was successfully used in photocells, rectifier diodes and solar cells. In its amorphous form, selenium has a good application as photoreceptor in copying machines and X-ray imaging plates [1,8,11].

Despite the increasing commercial using of a-Se in various applications (see [8] and references therein), e.g. as promising X-ray flat panel detectors for medical purposes [1], its structure is not fully understood.

On the other hand, binary non-crystalline semiconductors of As-Se system are also of continued scientific and practical interest because of real opportunity of their technological uses (e.g. as functional elements of multi-layer photoreceptors in xerography). Among them the stoichiometric composition, As_2Se_3, and compositions from the range 30-50 at % As are perhaps the most studied ones [12-19]. As for a most of stable binary glasses in As-Se system atomic ratios can be varied in a wide range. Although the information about various physical properties of Se-rich alloys is not so extensive and numerous [5-8,15-20], their compositional dependence manifests extrema or thresholds also in the range 6-12 at % As. It is necessary to accentuate that the As-Se amorphous alloy system display main extrema of various properties at the composition where the valence requirements appear to be satisfied that is at the stoichiometric composition. It seems to be reasonable to connect the mentioned non-monotonic behavior with a specific character of local structure changes.

Another prominent feature of the materials studied consists in the following. Certain type of glasses whose common feature is the presence of chalcogen atoms, sulfur, selenium, and tellurium, exhibit various photoinduced phenomena (the reader may refer to K.Shimakawa [10] and Ke.Tanaka [21]). Among these are photostructural transformations and photocrystallization phenomena: a change in optical, electrical and other physical properties is observed. The phase transformation of selenium and its alloys can also be induced relatively

simply by laser illumination [22-26]. Reasonably, this unique property makes them attractive for optical data storage and holographic recording. Many experimental results using selenium and its alloys have been reported [27], but few cases of phase transformation properties were mentioned.

In the present paper electron diffraction and Raman scattering in pure amorphous selenium (a-Se) and Se-rich As-Se amorphous films are studied. Below we attempt to clarify the structural transformations induced by light treatment and compositional changes. We focus our attention mainly on photocrystallization transformations. The article also deals with the composition induced structural modifications in amorphous As_xSe_{1-x}. As shows the analysis of electron diffraction and Raman scattering data, some discontinuity of atomic arrangement with rising As content exists.

2. Techniques exploited in structural studies

Methods used for structural study of solids may be classified into two groups.

1. Direct methods include diffraction of X-Rays, electrons and neutrons.

2. Among indirect methods Raman scattering, infrared absorption, extended X-Ray absorption fine spectroscopy and nuclear magnetic resonance can be considered.

The first ones are the methods of determining the arrangement of atoms within a solid, in which a beam of X-rays strikes a crystal and diffracts into many specific directions (Fig. 1). From the angles and intensities of these diffracted beams, a crystallographer can extract information about the mean positions of the atoms in the solid, as well as their chemical bonds, their disorder.

Since many materials are solids - such as semiconductors, as well as various inorganic, organic and biological molecules - X-ray crystallography has been fundamental in the development of many scientific fields. In its first decades of use, this method determined the size of atoms, the lengths and types of chemical bonds, and the atomic-scale differences among various materials, especially alloys. X-ray crystallography is still the chief method for characterizing the atomic structure of new materials.

It should be noted here that while diffraction of X-Rays, electrons or neutrons gives definite information about the structure of crystalline solids, such measurements give much less information about the structure of amorphous solids [28,29]. The diffraction patterns of amorphous solid consists of diffuse rings whose radial variation of intensity provides a merely one-dimensional representation of the three-dimensional glass structure. Some information about the structure is "averaged out" in the experiments and the structure is surely not 1-1 with the diffraction data. In practice one imagines a likely amorphous structure, predicts experiment and compares with the observation.
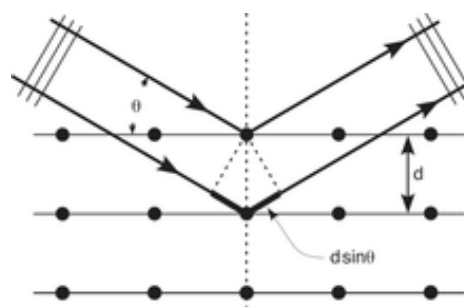

Fig. 1. Illustration of X-Ray diffraction from solids. The incoming beam causes each atom to re-radiate a small portion of its intensity as a spherical wave. If atoms are arranged symmetrically with a separation d, these spherical waves will be only in directions where their path-length difference 2d sin θ equals an integer multiple of the wavelength λ. In that case, part of the incoming beam is deflected by an angle 2θ, producing a reflection spot in the diffraction pattern.

This illustrates the need for the use of many different experimental probes. Diffraction, vibrational spectroscopy and other techniques emphasize different aspects of structure, such as interatomic distance, or angles, or local symmetry, or range of order. Each technique provides an alternative view of the structure and generally averages the structure differently, thus revealing aspects that may be de-emphasized or obscured by another technique. Although each probe gives limited information, the results of several different probes leading to a conviction of truth.
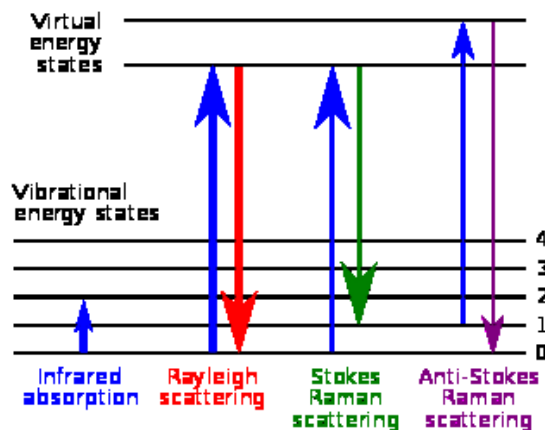

Fig. 2. Visible light scattering from molecules

Raman spectroscopy (named after C. V. Raman) is a spectroscopic technique used to study vibrational, rotational, and other low-frequency modes in a system. It relies on inelastic scattering of monochromatic light, usually from a laser in the visible, near infrared, or near ultraviolet range. The laser light interacts with phonons or

other excitations in the system, resulting in the energy of the laser photons being shifted up or down (Fig. 2). The shift in energy gives information about the phonon modes in the system.

Raman scattering is known to be a powerful technique which give information about local structure of amorphous chalcogenides [30,31].

3. Effect of composition on structure of As_xSe_{1-x} amorphous films – electron diffraction study

In the following experimental results of electron diffraction and electron microscopic measurements of the structure of As_xSe_{1-x} amorphous films are considered [27,32]. The results of structural investigations of films with low As content have been compared with the literature data.

The samples used in these studies were amorphous films, about 10 μm thick, prepared by vacuum thermal evaporation of the powdered As_xSe_{1-x} melt-quenched material at the rate of 1 μm/min. Freshly cleaved KCl single crystals on the (001) plane were used as substrates. The As_xSe_{1-x} bulk glasses were prepared according to the conventional melt-quenching method with agitating the ampoules content for homogenization. Annealing of the films was carried out in air at ambient pressure and at temperatures 40, 45, 50, 60, and 70 degrees (in Celsius scale) for 0, 2, 5, 10, and 20 at% As, respectively. The composition of the films was determined by electron probe microanalysis, and the composition quoted are accurate to within ± 0.5 at.%. Thin film samples were kept in complete darkness until measured to minimize exposure to light sources, which could lead to changes in the properties and structure of the films. Thermal evaporation method was used due to necessity of reproducing films with chemical composition of glasses. Moreover, the evaporation of As-Se glasses is not of a dissociate character, but it proceeds with fractionation [4]. The temperature T_{ev} of an open-type tantalum evaporator, measured with Pt/Pt-Rh thermocouple, was within $670 \leq T \leq 770$ K depending on glass composition.

The chemical composition of amorphous films was checked by X-Ray spectral microprobe method using the EMMA-4 instrument with a relative error ± 1 %.

The atomic structure of a film and its changes with thermal annealing were investigated by the electron diffraction method using the EMP-100 instrument and the microstructure was investigated in the EMB-100 B transmission electron microscope. It is necessary to note here that the film thickness for structural investigations did not exceed ~ 600-700 Å. The short-range order parameters of the atomic film structure were obtained by calculating the radial distribution function (RDF). The dependence $I = f(s)$, where $s = 4\pi \sin\theta / \lambda_e$, θ is the diffraction angle and λ_e is the wavelength of electrons, was plotted in a direct electron current recording mode.

The data about the character and changes in the medium-range order of the atomic film structure were measured by the analysis of positions and intensity of the first sharp diffraction peak (FSDP). The thermal annealing of films was carried out in situ, in the electron diffractometer column.

X-Ray spectral microprobe data of the film composition was the same as that of the As_xSe_{1-x} initial glasses (within the measurement error). This similarity showed that quasi-equilibrium evaporation conditions were maintained.

The electron diffraction patterns for As_xSe_{100-x} as-deposited amorphous films at x = 0, 2, 4, 6, 8, 10 and 40 are given in Fig. 3. For comparative analysis we plotted I / I_2 intensity curves, where I_2 is the intensity of the second peak of $I(s)$ curve which is less affected by the natural ageing of films [32].
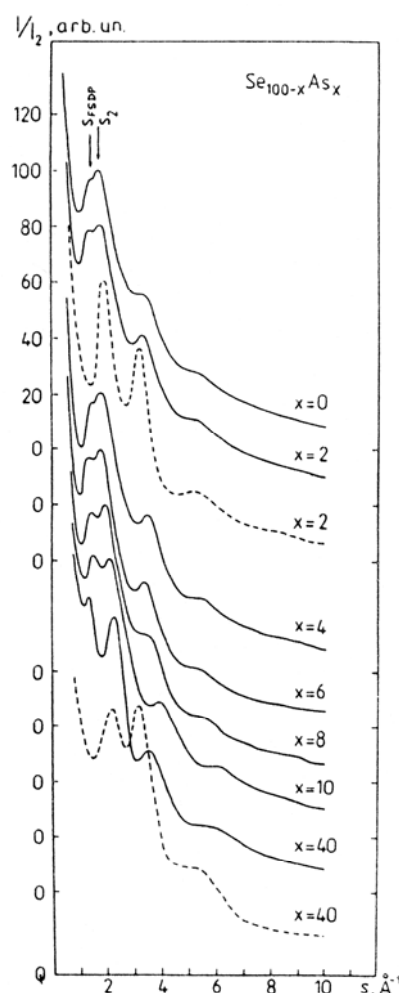

Fig. 3. Electron diffraction patterns of As_xSe_{100-x}As-deposited amorphous thin films (solid line) and films after structural transformation (dashed line) stimulated by thermal annealing

As clearly seen from Fig. 3, the presence of FSDP in the region $s_{FSDP} \approx 1-1.5$ Å is characteristic of

diffraction patterns for as-deposited films, and is associated [33-35] with medium-range order of the structure.

The data on the analysis of the first sharp diffraction peak position, s_{FSDP}, and the second peak, s_2, and their intensities, I_{FSDP} and I_2, for different compositions of As_xSe_{100-x} amorphous films are given in Figure 4. Here rounded and square symbols represent the distribution in values of data (for measurements on films prepared with the same evaporation parameters) for compositions with x = 0, 5 and 10. As seen from Fig. 4, the reproducibility of the parameters, s_{FSDP}, s_2, I_{FSDP} and I_2 for different evaporation conditions for films of the same composition is comparatively good.

After thermal annealing of films *in situ* (in the electron diffraction column), we observed a structural transformation, $A_1 \rightarrow A_2$, with retention of the amorphous state, where A_1 and A_2 were the phase state before and after transformation, respectively. Upon further heating, the films crystallized.
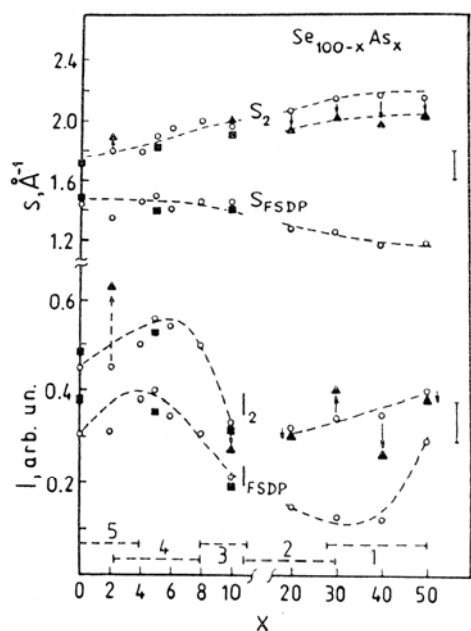

Fig. 4. Compositional dependence of S_{FSDP}, S_2, I_{FSDP} and $I_2$for amorphous As_xSe_{100-x} amorphous films. Solid circles and squares are referred to different deposition conditions; solid triangles and open symbols referred to S_2 and I_2 after $A_1 \rightarrow A_2$ structural transformation. Lines are guide for eyes.

The $A_1 \rightarrow A_2$ structural transformation in amorphous chalcogenide films is accompanied by a drastic change in the absorption contrast of the electron microscopic image. The main difference of diffraction patterns between films in the A_2 and in A_1 state lies in a complete disappearance of T_0 transition for the first sharp diffraction peak, I_{FSDP},

at a certain temperature. In Fig. 3, typical diffraction patterns of $As_{40}Se_{60}$ and As_2Se_{98} amorphous films after $A_1 \rightarrow A_2$ structural transformation are shown by dashed lines. New values of s_2 and I_2 for diffraction patterns As_xSe_{100-x} amorphous films of different compositions after $A_1 \rightarrow A_2$ transformation are shown in Figure 4 by triangular symbols.

It should be noted that diffraction patterns of As_xSe_{100-x} films with low As content after annealing are very similar to those of Se bulk glassy samples. This fact is in agreement with the results of refs. [31,36] in which authors show that the structure of As_xSe_{100-x} deposited films after annealing approaches that of corresponding glasses.

After thermal annealing of As_xSe_{100-x} amorphous films with compositions x ≤ 10, the $A_1 \rightarrow A_2$ structural transformation occurs even with slight heating caused by electron beam of instrument and films then crystallized. The recording of diffraction patterns for such films in the amorphous state after $A_1 \rightarrow A_2$ transformation is difficult.

In Fig. 5 the RDFs of As_xSe_{100-x} amorphous films for x ≤ 10 are given, and in Fig. 6 the data on the values of the first RDF maximum position, r_1, and area under it, z_1, are brought together. The values of r_1 and z_1 for films with x=30, 40 and 50 are given for comparison. The designation of the experimental points in Figure 2.6 corresponds to similar designations in Fig. 4.
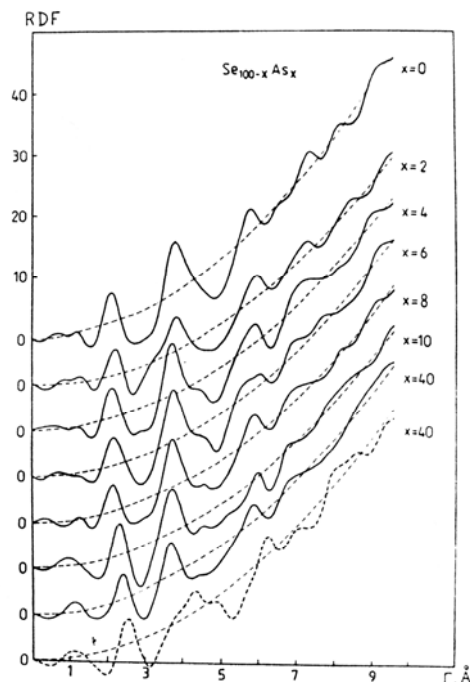

Fig. 5. Radial distribution functions (RDF) of As_xSe_{100-x} as-deposited amorphous films (solid lines) and films after structural transformation (dashed lines) stimulated by thermal annealing.
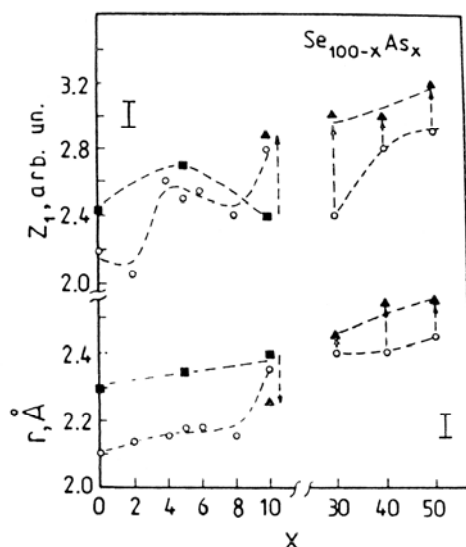
Fig. 6. Compositional dependence of the first RDF maximum position, r_1, and area under it, z_1, for $As_x Se_{100-x}$ amorphous films

4. Raman scattering in pure and alloyed amorphous selenium: high- frequency spectral region

Raman scattering is a very powerful experimental technique for providing information on the constituent structural units in a given material [30]. In the present section the Raman scattering in pure amorphous selenium (a-Se) and Se-rich As-Se amorphous films are studied. Below we attempt to clarify the structural transformations induced by light treatment and compositional changes. We focus our attention mainly on photocrystallization transformations. In addition, the composition induced structural modifications in amorphous $As_x Se_{1-x}$ are also analyzed. As shows the detailed analysis of Raman data, some discontinuity of atomic arrangement with rising As content exists.

The samples used in these studies were amorphous films, about 10 μm thick, prepared by vacuum thermal evaporation of the powdered $As_x Se_{1-x}$ melt-quenched material at the rate of 1 μm/min onto quartz substrates held at room temperature as well as polished mirror-like parallelepipeds of vitreous $As_x Se_{1-x}$. The $As_x Se_{1-x}$ bulk glasses were prepared according to the conventional melt-quenching method. Annealing of the films was carried out in air at ambient pressure and at temperatures below the glass-transition temperature. Thin film samples were kept in complete darkness until measured to minimize exposure to light sources, which could lead to changes in the properties and structure of the films. It is important accentuate that after annealing procedure their Raman spectra become indistinguishable from the corresponding spectra of melt-quenched glassy samples. It should be noted that for Se-rich compositions studied only slight difference in the spectra of melt-quenched and as-deposited samples is observed.

Right-angle Raman spectra were measured using RAMANOR U-1000 spectrometer. The spectral slit width was ~1 cm^{-1} and the excitation wavelength 676 nm. Raman spectra of the amorphous films were recorded with sufficiently low incident laser-beam power densities P=3 to 5 mW to avoid photostructural changes. The latter is known to transform the Raman spectra. The identity of the experimental spectra obtained from different points of the sample and the good reproducibility of the spectra in repeated scans (the time required to scanning one spectrum in the spectral range 100-300 cm^{-1} is about 5 min) show that photodarkening did not play a role in the subsequent Raman measurements.

The structure of photo crystallized films was investigated using X-ray diffraction.

It is important accentuate that after annealing procedure their Raman spectra become indistinguishable from the corresponding spectra of melt-quenched glassy samples. It should be noted that for Se-rich compositions studied only slight difference in the spectra of melt-quenched and as-deposited samples is observed.

Right-angle Raman spectra were measured using RAMANOR U-1000 spectrometer. The spectral slit width was ~1 cm^{-1} and the excitation wavelength 676 nm. Laser

The medium-range order of the structure of amorphous films may be characterized to a certain extent by values of s_{FSDP} and I_{FSDP}. From the analysis of Figure 4, it follows that $As_x Se_{100-x}$ as-deposited films in the region of compositions $0 \leq x \leq 10$ and $20 \leq x \leq 50$ differ in a correlation length, $L = 2\pi / s_{FSDP}$, of the medium-range order and in the degree of medium-range ordering.

The FSDPs for amorphous films of composition close to $As_{40}Se_{60}$ are explained in the approximation of the cluster model. According to this model the correlation length, L, is associated with the size of quasi-molecular (cluster) species in the structure of as-deposited films [37].

In the region of low As content, the calculated values of correlation length are $0.42 \leq L \leq 0.46$ nm, whereas for the region of compositions $30 \leq x \leq 50$ one obtain $0.50 \leq L \leq 0.55$ nm. The latter is fairly well fitted [38] with the distance between the "furthest" Se atoms in $As_n Se_m$ quasi-molecular species (n=4, m=6). The average value of L in the compositional range $0 \leq x \leq 10$ correlates with the sizes of Se_6 molecules and with the average distance between Se_n chains in the structure of amorphous selenium [4].

We suppose that the peculiarities observed in compositional dependence of structural characteristics for $As_x Se_{100-x}$ films with low As content are conditioned by a topological structure of the disordered network to appear just in those local regions where linking, branching of chains and formation of closed rings occur. In practice, this fact results in an increase in the intensity of the main diffraction peak I_2 and peak I_{FSDP} being responsible for the medium-range order, and in a mutual change in the position of these peaks.

beam is focused into 100 μm spot. Raman spectra of the amorphous films were recorded with sufficiently low incident laser-beam intensity $I=1.3\times10^2$ W/cm^2 to avoid photostructural changes. The identity of the experimental spectra obtained from different points of the sample and the good reproducibility of the spectra in repeated scans (the time required to scanning one spectrum in the spectral range 100-300 cm^{-1} is about 5 min) show that photodarkening did not play a role in the subsequent Raman measurements.

In Fig. 7, a typical Raman spectrum of a-Se measured at low incident radiation power density, ~3 mW, is shown. The stable level of the scattered light intensity and the good reproducibility of the spectrum in the repetitive cycles clearly indicate the absence of any structural changes in a-Se induced by laser irradiation of such power density. On the high-frequency side (ω=100 to 300 cm^{-1}) the spectrum contains an intensive peak at 255 cm^{-1} and some peculiarity (shoulder) at 237 cm^{-1}.
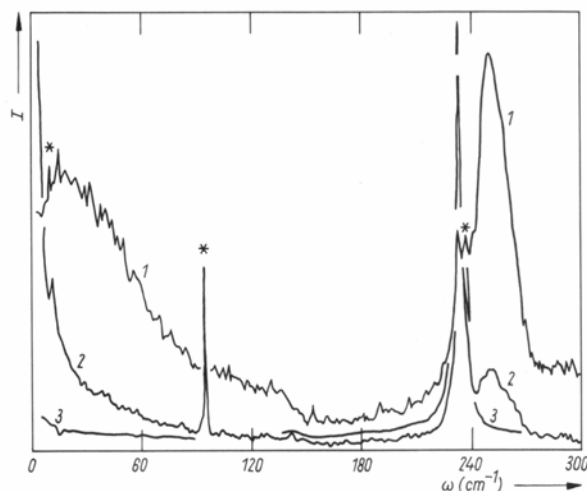

Fig. 7. Raman spectra of (1) amorphous and (2), (3) photocrystallized selenium. Experimental details for (2) and (3) are: (2) after 5 min exposure of the sample to 10 mW, (3) after 30 min exposure to 10 mW. Asterisks indicate laser plasma lines.

The above features are in good agreement with previously reported data [39-43]. In the low-frequency region one can observe the broad peak with ω_{max}=16 to 20 cm^{-1}. This so-called boson peak occurs in the low frequency region of the Raman spectra of all amorphous and vitreous solids. We considered this spectral region in separate paragraph.

When we try to identify certain vibration bands observed in the Raman spectrum of a-Se, some difficulties arise. Initially it was proposed to interpret the a-Se Raman spectrum by analogy with sulfur – on the basis of a molecular approach. That is, the main vibration band was considered to be the superposition of the peaks at 237 and 255 cm^{-1} characteristic of chains and rings, respectively [41]. However, further experimental data have caused

some doubts to be cast. In such a case one would expect to observe a discernible difference in the contributions of 237 and 255 cm^{-1} modes to the main vibration band in the samples prepared at different conditions (e.g. substrate temperature during deposition for amorphous films or quenching rate for glassy samples). This may be caused by changes in rings to chains ratio. Therefore, it is clear that the spectral region 200 to 300 cm^{-1} is unsuitable for ring diagnostics. This is consistent with the conclusions of [42].

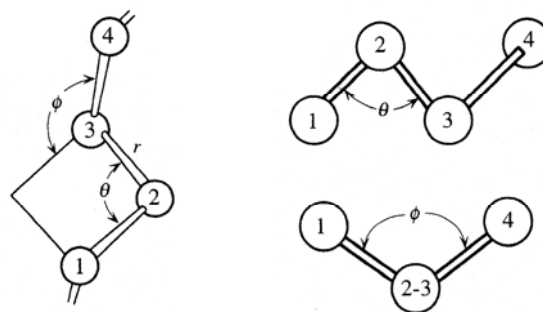
Fig. 8. Se chain molecule and definition of the dihedral angle ψ. The definition involves an angle between planes and thus four atoms labeled 1, 2, 3 and 4. It is observed looking down the bond joining atoms 2 and 3.
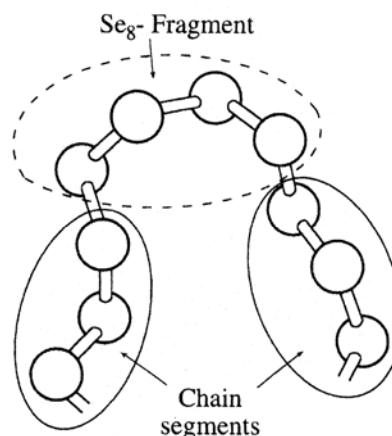

Fig. 9. Local molecular order in a selenium chain in which there are segments characterized by repetition of the same dihedral angle ("chainlike" in the sense of trigonal Se) and segments characterized by alternating dihedral angle ("ringlike" in the sense of Se$_8$ molecule)

The Se$_8$ peak (112 cm^{-1}) could not be detected in the present experiment. Probably, this is connected with its weakness. This fact indicates evidently the low concentration of rings. Consequently, one can associate the spectral features in the main vibration band, the 255 cm^{-1} peak and the shoulder at 237 cm^{-1}, mainly with the chain vibrations.

In the present section experimental results on Raman scattering spectra for Se-rich amorphous semiconductors As_xSe_{1-x} are also discussed. In Fig. 10 typical Raman spectra of amorphous Se and As-Se alloys with As content up to 5 at % are shown. The major spectral feature in the high-frequency region is the 255 cm^{-1} band. Another prominent spectral feature which is not shown in this Figure is the broad peak at ω_{max}=16÷20 cm^{-1}. As mentioned, the latter is characteristic for Raman scattering of all amorphous solids and glasses.

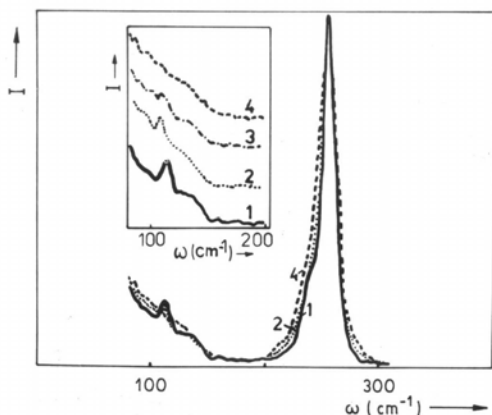*Fig. 10. Comparison of the Raman spectra of (1) amorphous Se and As_xSe_{1-x}: (2) x=0.02, (3) 0.04, and (4) 0.05 at %. Each trace has been normalized to the same peak (255 cm^{-1}) intensity. The inset shows the bending mode region.*

In the following we consider only the high-frequency region. The weak feature observed at 112 cm^{-1} in the a-Se spectrum diminishes with As addition and at 5 at % completely disappears (see inset Fig. 10). At the same time the difference in the spectra in the region of the main vibration band is obvious. Thus, with increase of As content the transformation of the Raman spectrum in this region is retraced (Fig. 11).
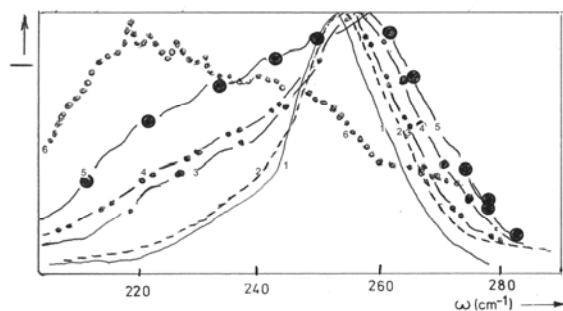

Fig. 11. Raman spectra of amorphous As_xSe_{1-x} films annealed at T=Tg. (1) x=0 (solid line), (2) 0.05 (dashed line), (3) 0.10 (dashed-doted line), (4) 0.12 (dashed-double doted), (5) 0.20 (solid circles), and (6) 0.40 (points). We have used these unconventional denotations for Raman spectra to be distinguishable.

The most important points are the following.
1.   Spectrum broadening with increasing As addition.
2.   Growth of scattered light intensity from the low-frequency side of the main maximum (255 cm^{-1}).
3.   Appearance of a broadened band at 220÷230 cm^{-1} (this band is the most intense in the Raman spectrum of $As_{0.4}Se_{0.6}$). It should be noted also that the main maximum is slightly shifted to higher frequency for amorphous As_xSe_{1-x} respectively to Se (255cm^{-1}).

The intensity of the 220÷230 cm^{-1} band in the As concentration interval 0-5 at % remains practically unchanged. Then, at 6 at % As, an increase of the band intensity occurs. A gradual intensity rise is observed for the band at 220 cm^{-1} as the As content is further increased. For As content exceeding 35 at % the band dominates in the Raman spectrum.

It seems to be reasonable to approximate the observed Raman spectra of As_xSe_{1-x} as superposition of the spectra of amorphous Se and $As_{0.4}Se_{0.6}$. The corresponding calculations have been performed. These calculations yield that a systematic discrepancy between approximated and experimental spectra is observed. As for the latter, the greater values of the main peak width are typical.

Fig. 12 shows difference spectra obtained by subtracting the $As_{0.4}Se_{0.6}$ spectrum from experimental Raman spectra. The relative contribution of the $As_{0.4}Se_{0.6}$ spectrum was fitted to the ~230 cm^{-1} region where the contribution from pure Se was negligibly small. It is obvious that after such a procedure some peak remains, width and position of which differs from that for a-Se. Based on the data given in Fig. 12, values of the parameter A were estimated. This parameter represents the ratio of the integrated Raman intensity in the interval limited by the typical frequencies of $AsSe_{3/2}$ unit vibrations (205 to 230 cm^{-1}) to the integrated intensity of the whole spectrum of valence vibrations: $A = \int_{205cm^{-1}}^{230cm^{-1}} I \ / \int_{205cm^{-1}}^{290cm^{-1}} I$ (here I is the intensity of the corresponding Raman band). Figure 2.13 shows that the dependence $A \sim f(x)$ is non-monotonous – parameter A increases around ~ 6 at % As. For the frequency range 240 to 270 cm^{-1}, the change of scattered intensity with composition has a smoother character. On the same figure, the dependence of the peak frequency, ω_{max}, and its width, $\Delta\omega_{max}$, on As content for the corresponding spectra is displayed. It is important to note the similarity of the composition dependence of A, ω_{max}, and $\Delta\omega_{max}$.

An attempt to simulate As_xSe_{1-x} Raman spectra by a superposition of two constant spectral forms one of which belongs to a-Se, the other to $As_{0.4}Se_{0.6}$ failed. Onari et al. [44,45] was first who used a similar approach. On the contrary, the experimental spectra could be approximated assuming a considerable broadening of chain vibrations and their frequency displacements. We consider that such an approach is correct and that the difference spectra themselves are convincing arguments in favor of it: the change of the Raman spectra with composition together

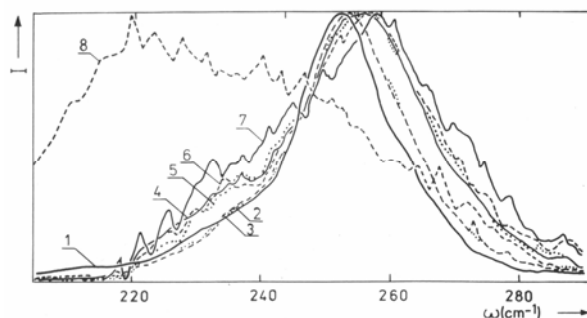with parameters A, $\omega_{max,}$ and $\Delta\omega_{max}$ (see the corresponding figures) support this suggestion.

Fig. 12. The difference spectra (see the text for details) for a-As_xSe_{1-x}. x=0.04, 0.05, 0.06, 0.08, 0.10, and 0.20 at %, curves 2 to 7, respectively. For the sake of comparison Raman spectra (1) of a-Se and (8) $As_{0.4}Se_{0.6}$ are also shown.

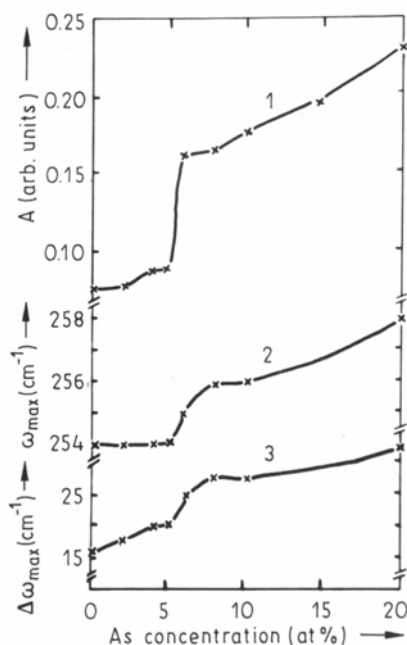*Fig. 13. Composition dependence of the parameters (1) A, (2) ω_{max}, and (3) $\Delta\omega_{max}$*

Composition-dependent studies on the physical properties of binary and ternary chalcogenide glasses give evidence for the existence of mechanical and chemical thresholds at certain compositions of these materials [46-48]. The As-Se system displays main extrema of various properties at the stoichiometric composition (the mechanical and chemical thresholds coincides at x = 0.40). There seem to exist (see experimental results published by Kasap [49] and present data) an additional threshold at $0.06 \leq x \leq 0.12$. It can be argued that the non-monotonic behavior observed in the concentration dependence of glass transition temperature, density, etc [50] in this range

originates from changes in bond topology [46,49]. We assume that in Se-rich glasses the network is dominated by Se atom chains (quasi-one-dimensional network) and addition of As atoms lead to branching owing to threefold coordination of As atoms. Recent publications [49,51,52], as we believe, give a new approach to the problem of local bonding in amorphous chalcogenides. The anomalous behavior near x ≈ 0.06 is ascribed to the disappearance of Se_8-like segments. From the point of view of configuration, it is suggested that the number of *cis*-configurations in rings starts to decrease, so that the mediate-range correlation is modified. The considerable reduction in the vibration mode at ~112 cm^{-1} associated with *cis*-segments in ring component strongly supports this suggestion.

Changes in the Raman spectrum with composition allow us to conclude that incorporation of As leads to cross-links between chain-like or ring-like segments of amorphous Se.

There are strong indications that the compositional dependence of physical and chemical properties has no connection with chemical ordering. In fact, the binary As_xSe_{1-x} alloys exhibit extrema in compositional dependence of the density not only at the $As_{0.4}Se_{0.6}$ composition, but also for the non-stoichiometric chalcogen-rich $As_{0.06}Se_{0.94}$ and also for pnictogen-rich $As_{0.6}Se_{0.4}$ samples. This means that the x dependence of the density originates from changes in bonding topology.
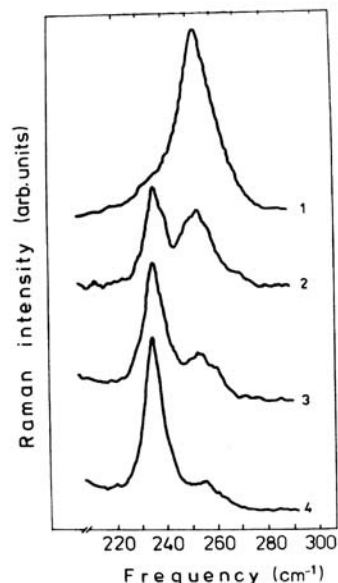

Fig. 14. Laser-induced transformation of Raman spectra of amorphous Se. Experimental details for (1)-(4) are: (1) reference spectrum of amorphous state, (2)-(4) after exposure to E = 3.8, 11,4 and 19 × 10^3 J/cm^2, respectively. I = 1.3 × 10^2 W/cm^2.

We may summarize the general features of the observed transformation of Raman spectra in the range of bond bands for amorphous selenium. 1) There is (Fig. 14) a certain threshold energy, E_{th}, of the incident radiation. 2)

Below E_{th}, no changes of Raman spectrum are observed. Here we note that the only exception is the so-called boson peak detected at around 17 cm^{-1} which is weakened by illumination. 3) Above E_{th}, an increase of the incident energy density modifies the spectra.

The present experimental results permit to distinguish three successive stages of photocrystallization in a-Se with regard to irradiation energy density. First of all it is necessary to point out the absence of any significant structural transformations in films and bulk samples at $E_{th} \leq 4$ J/cm^2. This is strongly supported by the identity of the Raman spectra recorded in repetitive cycles. At the first stage, which is induced by irradiation with incident energy density ≥ 3.8 J/cm^2, microcrystallite formation probably takes place. In such a case the 255 cm^{-1} peaks dominates the Raman spectra.

The second stage of photocrystallization (~ 11 J/cm^2) is characterized by an enlargement of microcrystalline units. This is demonstrated by the growth of the 237 cm^{-1} peak. Finally, at ~ 20 J/cm^2, photocrystallization practically takes place. This stage is marked by a dramatic increase and narrowing of the peak at 237 cm^{-1} with irradiation time. At the same time, the 255 cm^{-1} peak becomes more and more suppressed with respect to other Raman active modes and, finally, it completely disappears. At this last stage of photocrystallization the absence of the low frequency (17 cm^{-1}) peak is also characteristic.

It seems to be reasonable to assume a thermal, caused by laser heating of the sample, mechanism for the observed structural transformation. This suggestion is strongly confirmed by the clearly manifested threshold behavior. Additional support comes from the fact that at low temperature the threshold power (e.g. 20 J/cm^2 at T=100 K for a-Se) which is necessary for changes in Raman spectra to be observable exceeds several times that for changes at T=300 K. Note that the changes under examination qualitatively differ from the well-known photodarkening phenomena. As for the latter, it takes place at any value of irradiation power; threshold behavior was not characteristic of them. The magnitude of photodarkening depends mainly on the amount of absorbed energy and significantly increases with temperature lowering.

The relatively greater efficiency in films in comparison with bulk samples is established feature of photodarkening. In contrast, in our case, the threshold power densities for a-Se films are found to be higher than for bulk samples. According to results [53,54], discernible, reversible photodarkening in a-Se at T=100 K occurs at photon energy hv ≥ 2.0 eV with efficiency maximum at ~ 2.4 eV. Probably, the exciting irradiation energy, hv=1.84 eV seems to be low to induce significant photodarkening at T=100 K. At the same time the probability of transient photodarkening effects relaxing after finishing the irradiation at T=300 K for E ≈ 3.8 J/cm^2 cannot be definitively ruled out.

With regard to As$_x$Se$_{1-x}$ Raman data, principal results are the following:

1.   The spectra of the As$_x$Se$_{1-x}$ amorphous alloy samples before irradiation were the same as those reported in Refs [15, 31, 40, 42, 43-45].

2.   The value of E_{th} necessary for changes in Raman spectra to be observable vary with addition of As (see Table 1 given below)

3.   Under irradiation with E>E_{th} the recorded spectra clearly show a narrowing and increase in the intensity of the 237 cm^{-1} Raman band.

4.   In As$_x$Se$_{1-x}$ samples with x≤ 0.05, no additional (to that recorded for pure Se) photoinduced changes in their Raman spectra are observed (see Fig. 15 and compare with the results for a-Se). It should be accentuated that, on introducing such a relatively large quantity of As additives, there is no appreciable influence on the photocrystallization product. It is well known that Se is likely to be photocrystallized at ~ 350 K [22, 50]. Reasonably, X-ray diffraction patterns of the samples have been measured. Since the illumination region is of ~ 3mm in radius, the pattern is noisy. However, we can clearly see four crystalline peaks located at $2\theta = 24^o$, 30°, 41°, and 45°. The peaks can be indexed, respectively, as 100, 101, 110, and 111 of the trigonal (hexagonal) Se crystal [55].

5.   For As content >15 at%, the main result of this study is the appearance and disappearance of new Raman bands typical for As$_{0.4}$Se$_{0.6}$.

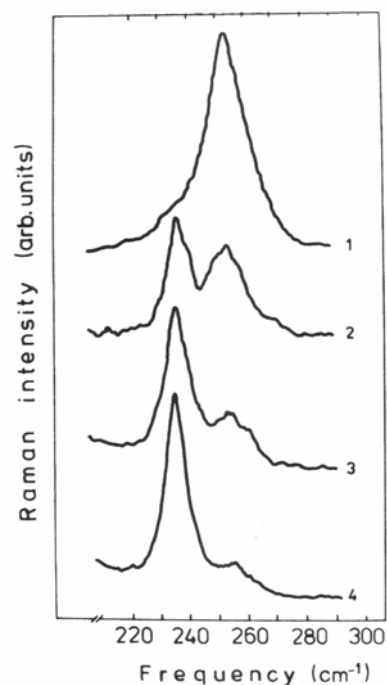*Fig. 15. Development of the photocrystallization effect in As$_{0.05}$Se$_{0.95}$ as a function of exposure: 1, reference spectrum of amorphous state; 2, 3, after exposure to 15 and 25×10^3 J/cm^2, respectively. I = 1.3×10^2 W/cm^2.*

Table 1. E_{th} values as a function of As concentration in As_xSe_{1-x} alloys

As concentration (at %):	0	5	8	12	20
E_{th}^* (kJ/cm^2) :	2±1	12±3	7±2	8±2	45±5

* The E_{th} values are shown for the case I=1.3×10^2 W/cm^2

For example, Fig. 15 shows the appearance of an additional peak (~264 cm^{-1}) superimposed on the amorphous peak (~255 cm^{-1}). With a further increase of the irradiation energy density, crystallization starts immediately. Here we should note an evolution qualitatively similar to that shown for pure Se and $As_{0.05}Se_{0.95}$ in the shape of spectra over the concentration range 0-20 at %. In the final stage of photocrystallization, the spectra of As_xSe_{1-x} alloys are free of key crystalline features that occur [56] in the spectra of crystalline As_2Se_3. It is of particular significance that only the 237 cm^{-1} band of trigonal selenium contributes to the spectra of photocrystallized As_xSe_{1-x} (0<x<20) films.

We define E_{th} (e.g. E_{th}=2×10^3 J/cm^2 at I=1.3×10^2 W/cm^2 in the case of pure Se) as the energy density for which the system is not yet perturbed structurally (on the scale of short-range order) by laser irradiation. The absence of any significant bonding changes in films is supported by the identity of the Raman spectra recorded in repetitive cycles. This result holds for both pure amorphous selenium and Se-rich As_xSe_{1-x} alloys. For energies less than E_{th} reversible photodarkening and transient transmission changes are observed. These effects are characteristic of the amorphous phase and the system remains in the amorphous phase under or even after irradiation. The lack of any noticeable variation in the transient behavior T_{rel} for samples of different substrate material and film thickness exclude the possibility of the effect being due to small changes in sample temperature during and after illumination, i.e., to photoinduced heating.

We have recently reported similar dynamical photoinduced changes in some photoelectronic properties detected by time-of-flight and xerographic technique [18-20, 57]. These experiments may provide the first evidence that deep defects can be altered temporarily by room-temperature irradiation. Note that there is a close correlation between the recovery of optical parameters and photoelectronic characteristics in exposed samples. Although a complete correlation of microscopic structural modifications with macroscopic photodarkening phenomena must await further experimental measurements, it is only natural that we relate the transient changes in the transmissivity with changes in deep defect states. We identify such centers as arising from native (thermodynamic) structural defects (e.g., C_3^+ and C_1^- in amorphous selenium). Band-gap light can probably initiate conversion of traps of small cross-section to those of larger cross-section [8,58].

By contrast, above E_{th}, all the observed irreversible changes may be attributed to optical constant variations and modifications in the kinetics of light-induced crystallization. The present experimental results resolve successive stages of photocrystallization in a-Se (these were mentioned above). In such a photocrystallization process, amorphous Se undergoes a transformation to the trigonal selenium which is the most stable modification. Raman scattering studies together with X-ray diffraction data gave an unambiguous indication of trigonal selenium.

On the basis of the present Raman data, we conclude that the features of the photocrystallization effects in As_xSe_{1-x} alloys with x<0.15 are qualitatively the same as those in amorphous selenium. Some deviation in pre-crystallization behavior of $As_{0.2}Se_{0.8}$, namely the appearance and disappearance of the weak quasi-crystalline peak at 264 cm^{-1}, probably indicates As_2Se_3-like cluster creation and annihilation. The latter could be clusters with a more ordered structure with respect to that existing in amorphous phase. At the same time, they are not yet microcrystallites with inherent Raman peaks. It seems to be reasonable that the environment of the clusters prevents their growth and transformation into microcrystallites. Other Se clusters reach the critical size required for microcrystallite formation. After that, sample exposure to E>E_{th} crystallized selenium, while the As-containing clusters remained in amorphous phase. The above explanation is in agreement with the results of the study of laser-induced structural transformations in glassy As_2Se_3 [58] and also with the mechanism proposed by Phillips [59].

It is known [50] that As is an effective additive to decrease the tendency to crystallization. Our experimental results, namely the greater value of E_{th} for a-As_xSe_{1-x} films, indicate that the addition of As effects the suppression of the crystal nucleation and growth in amorphous selenium. The long Se chains in amorphous selenium branch at the site of As atoms. The length of Se chains becomes short [45, 60] and the amorphous Se cannot easily crystallize with increase of As concentration.

At the same time, it is necessary to note that the changes in optical transmissivity and diffraction efficiency that occur are not monotonic with increasing As content. It seems to be reasonable to connect such a behavior with some discontinuity of atomic arrangement with increasing As content. Our recent study of composition dependence of Raman bands in amorphous As_xSe_{1-x} supports this suggestion.

5. Raman scattering in pure and alloyed amorphous selenium: low- frequency spectral region

It has become evident that traditional techniques of structural investigation are inefficient for study of disordered materials. They give information on the structure of a short-range order only and are slightly sensitive to more long-range correlations in arrangement of atoms. The existence of the medium-range order is admitted: periodic atomic arrangement inherent in crystals remains within several coordination spheres and

then is violated. It is assumed that the character of the violation may depend on preparation and chemical composition of the sample [28, 61]. A number of experimental procedures were proposed, for measurement of a size ordered microregions, or structural correlation range R_c. One of these methods permits to determine R_c by the position of a low-frequency boson peak in Raman spectra [62].

It has been shown [61-63] that the Raman intensity can be described by

$$I / \varpi (n(\varpi) + 1) = \sum_B c_b(\varpi) g_b(\varpi) / \varpi^2,$$

where $g_b(\varpi)$ is the density of states and $c_b(\varpi)$ is the matrix element of the coupling of the vibration mode b to the light, $n(\varpi)$ is the boson occupation number. In the low-frequency region $I / \varpi (n(\varpi) + 1) \sim \varpi^2$ increases and then reaches a maximum at certain value $E = E_{max}$ (Fig. 16), which depends on chemical composition and thermal prehistory of the sample [63, 64]. This peak was called in literature as a boson peak. It accounts for 30 to 90% of integrated intensity of Raman spectrum in glasses.

Authors [61] have compared spectral form of the low-frequency band in various samples. For the sake of simplicity all the spectra are given in the same energy scale $E_n = E / E_{max}$ (Fig. 17). A unique property of the boson peak was found: in a broad frequency range the form of the peak is independent of chemical composition of the sample. Additional analysis of results (Fig. 17) indicates that the boson peak has a universal nature, which is due to the most general features of vitreous structure and is not associated with the concrete chemical composition of glass or with the structure of corresponding crystal. One of these features is the medium-range order. Universal form of the boson peak is assumed to be due to this general character of vitreous solids.
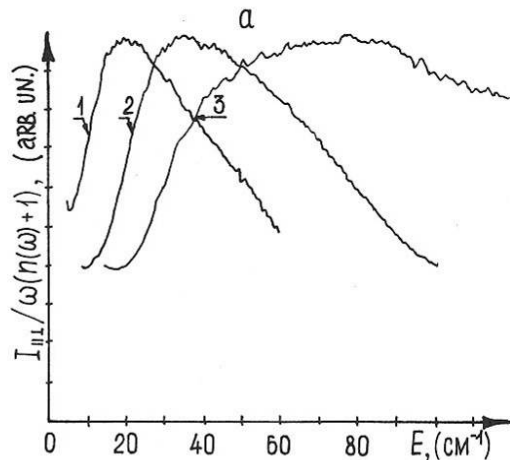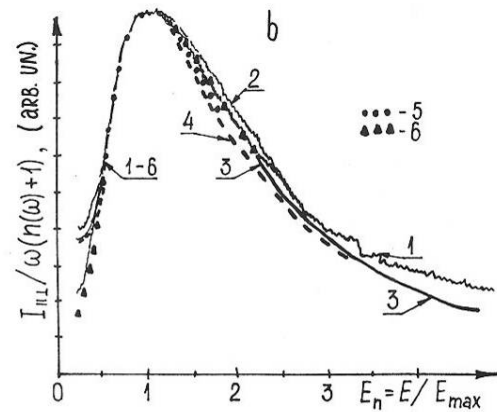

Fig. 17. Raman spectra of different glasses in a scale $E_n = E / E_{max}$: 1 – As_2S_3 ($E_{max} = 26$ cm^{-1}), 2 – $Bi_4Si_3O_{12}$ (34 cm^{-1}), 3 – SiO_2 (52 cm^{-1}). In addition it is shown spectra: 4 – B_2O_3 (28 cm^{-1}), 5 – B_2O_3O (45 cm^{-1}), 6 – GeS_2 (22 cm^{-1}) and 7 – Li_2O (88 cm^{-1}) [61]

The low frequency region $0 < \omega < 100$ cm^{-1}, in which the boson peak appears in a-Se, is of special interest. It has been found that the spectral form of the boson peak is nearly the same for a wide series of oxides, chalcogenides, and low-molecular organic glasses. The universal form of the low frequency peak is due to universality of glassy material in the scale of medium-range order L $\sim v/\omega_{max}=1$ to 2 nm (v is the sound velocity). For the case of a-Se, it is observed (Fig. 18) that the spectral form of the boson peak essentially differs from that characteristic of the majority of inorganic glasses. The spectral form of the boson peak in a-Se seems to be intermediate between that in polymeric and low-molecular glasses.

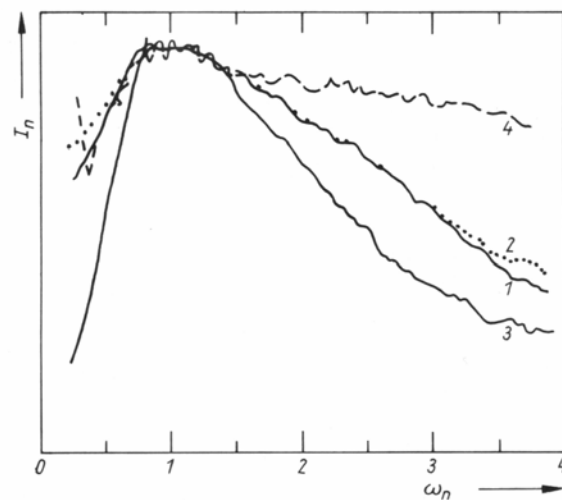Fig. 16. Low-frequency Raman spectra of As_2S_3 – 1, $Bi_4Si_3O_{12}$ – 2, $La_2S_3Ga_2S_3$ – 3 glasses [61]

Fig. 18. Low-frequency Raman spectra of different glasses in a scale $\omega_n=\omega/\omega_{max}$. (1) Se ($\omega_{max}=17$ cm^{-1} at T=100 K), (2) Se ($\omega_{max}=17$ cm^{-1} at T=300 K), (3) As_2Se_3 ($\omega_{max} = 26$ cm^{-1}, $T = 300$ K), (4) polymethylmetacrylate (PMMA) ($\omega_{max}=17$ cm^{-1}).

Normalized Raman spectra $I_n=I/\omega(n(\omega) + 1)$ for a-Se and series of other composition samples are given in the same energy scale $\omega_n=\omega/\omega_{max}$, where $n(\omega) + 1=1/(exp(h\omega/kT) - 1) + 1$ is the boson factor for the Stokes component.

This result can be explained by a preferentially chain-like structure of a-Se. The latter may form a structure similar to the structure of linear polymers PMMA. In other words, with regard to its structure on the scale of medium-range order, a-Se may be placed between 3-dimensional network glasses and polymeric ones. Examples of mediate-range order in elemental and compound materials, including a-Se, have been extensively discussed in [65-70].

There exists another possible explanation. Se has its glass transition temperature near room temperature; therefore it is in a well annealed state. It is known [61] that the intensity of the boson peak relative to the main bond modes in the Raman spectrum significantly decreases as the structural order of the sample increases (e.g. in "equilibrated" or annealed samples). This decrease in turn may lead, respectively, to an increased contribution from other modes to the high-frequency side ($\omega \geq \omega_{max}$) of the boson peak. This is clearly seen if we compare the shape of corresponding peaks in a-Se and As_2S_3 (Fig. 18).

6. Conclusions

The molecular structure of amorphous selenium differs from that of the majority of inorganic glasses on a scale of medium-range order. Apparently, Se chains form a structure similar to the structure of linear polymers on the scale ~1 nm.

Depending on the irradiation energy density, two qualitatively different regions are observed. Below the energy density threshold, E_{th}, only small changes in the local structure of the system can be detected.

Above E_{th}, the changes were attributed to crystallization transformation. In addition, we have detected the successive phases in such a transition which is a threshold phenomenon.

It has been shown that Raman scattering spectra of amorphous As_xSe_{1-x} alloys change non-monotonically with composition in the region of bond stretching modes. Certain extrema in various physical properties exist at composition range 6-12 at % As. The presence of this topological threshold is established by direct evidence, such as peculiarities in the compositional dependence of the Raman vibration modes of glasses. These peculiarities are caused by the transition from a chain-ring-like structure to chainlike structure with increasing degree of cross-linking.

Based on Raman scattering studies, we have shown how the structure transforms chronologically in amorphous As_xSe_{1-x} recording media.

Laser-induced changes at room temperature involve two phenomena essentially different in their origin: transient reversible changes (photodarkening) and irreversible changes (photocrystallization) with gross structural reorganization. For high values of energy density, the Raman spectrum has pronounced crystallization-related changes.

Our explanation are based on the assumption that the radiation pumps the material from an amorphous state towards the crystalline state through the formation of small clusters, which coalesce to form large clusters attaining microcrystallite size at high energy density levels.

References

[1] S. O. Kasap, J. B. Frey, G. Belev, O. Tousignant, H. Mani, L. Laperriere, A. Reznik, J. A. Rowlands, Phys. Status Solidi **B 246,** 1794 (2009).
[2] M. Popescu, J. Non-Cryst. Solids **352,** 887 (2006).
[3] A. Madan, M. P. Shaw, "The Physics and Applications of Amorphous Semiconductors" (Academic Press, Boston, MA, 1988).
[4] A. Feltz, "Amorphous Inorganic Materials and Glasses" (VCH, Weinheim, Germany 1993).
[5] V. I. Mikla, V. V. Mikla, J. Mater. Sci.:Mater. Electron **20,** 1095 (2009).
[6] V. I. Mikla, V. V. Mikla, J. Optoelectron. Adv. Mater. **10,** 131 (2008).
[7] V. I. Mikla, V. V. Mikla, Optoelectron. Adv. Mater. – Rapid Comm. **1,** 272 (2007).
[8] S. O. Kasap, in "Handbook of Imaging Materials" edited by A.S.Diamond and D.S.Weiss (Marcel Dekker, Inc., New York, Second Edition, 2002) p. 329, and references therein.
[9] K.Tanaka, in "Encyclopedia of Materials (Elsevier Science Ltd., 2001) p. 1123.
[10] K. Shimakawa, Advances in Physics **44,** 474 (1995).
[11] S. O. Kasap, J. A. Rowlands, J. Mater. Sci. Mater. Electron. **11** (2000) 179.
[12] Z. Borisova, "Glassy Semiconductors" (Plenum Press, New York, 1981).
[13] N. F. Mott, E. A. Davis, "Electronic Processes in Non-Crystalline Naterials" (Oxford University Press, Oxford, Second Edition, 1979).
[14] K. Hulls, P. W. Mc Millan, J. Non-Cryst. Solids **15,** 357 (1974).
[15] J. Schottmiller, M. Tabak, G. Lucovsky, A. Ward, J. Non-Cryst. Solids **4,** 80 (1970).
[16] A. E. Owen, A. P. Firth, P. J. S. Ewen, Philos. Mag. **B 52,** 347 (1985).
[17] A. E. Owen, W. E. Spear, Phys. Chem. Glasses **17,** 174 (1976).
[18] V. I. Mikla, D. G. Semak, A. V. Mateleshko, A. R. Levkulich, Sov. Phys. Semicond. **21,** 266 (1987).
[19] V. I. Mikla, D. G. Semak, A. V. Mateleshko, A. R. Levkulich, Sov. Phys. Semicond. **23,** 80 (1989).
[20] V. I. Mikla, J. Phys.: Condens. Matter **9,** 9209 (1997).
[21] K.Tanaka, Rev. Solid State Sci. **2&3,** 644 (1990).
[22] J. Dresner, G. B.Strinfellow, J. Phys. Chem. Solids **29,** 303 (1968).

[23] J. P. De Neufville, in "Optical Properties of Solids – New Developments" edited by D.O.Seraphin (North-Holand, Amsterdam, 1975) p. 437.

[24] H. Fritzsche, in "Insulating and Semiconducting glasses" edited by P.Boolchand (World Scientific, Singapore,2000) Chap 10.

[25] V. I. Mikla, I. P. Mikhalko, J. Non-Crystall. Solids **180,** 236 (1995).

[26] M.Chomat, D. Lezal, J. Gregore, I. Srb, J. Non-Crystall. Solids **20,** 427 (1976).

[27] V. I. Mikla, J. Phys.:Condens.Matter **9,** 9209 (1997).

[28] V. P. Zakharov, V. S. Gerasimenko. "Structural Peculiarities of Semiconductors in Amorphous State" (Naukova Dumka, Kiev, 1984).

[29] F. L. Galeneer, J. Non-Crystall. Solids **123,** 182 (1990).

[30] M. Cardona, "Light Scattering in Solids" (Springer-Verlag, Berlin, 1975).

[31] R. J. Nemanich,G. A. Connell, T. M. Hayes, R. A. Street, Phys. Rev. B **18,** 6900 (1978).

[32] O. V. Luksha, V. I. Mikla, V. P. Ivanitsky, A. V. Mateleshko, D. G. Semak, J. Non-Crystall. Solids **144,** 253 (1992).

[33] L.Cervinka, Czech. J. Phys. **B 25,** 1193 (1985)

[34] S. R. Elliott, J. Non-Crystall. Solids **106,** 26 (1988).

[35] J. S. Lannin, Phys. Today **41,** 28 (1988).

[36] A. J. Leadbetter, A.J.Apling, **21,** 47 (1976).

[37] A. C.Wright, R. N. Sinclair, A. J. Leadbetter, J. Non-Crystall. Solids **71,** 295 (1985).

[38] M. F. Daniel, A. J. Leadbetter, A. C. Wright, R. N. Sinclair, J. Non-Crystall. Solids **23,** 271 (1979).

[39] A. A.Baganich, V. I. Mikla, D, G, Semak, A. P. Sokolov, phys. Stat. Sol. (b) **166,** 297 (1991).

[40] M. Gorman, S. A. Solin, Solid State Commun. **18,** 1401 (1976).

[41] M. H. Brodsky, M. Cardona, J. Non-Crystall. Solids **31,** 81 (1978).

[42] P. J. Carroll, J. S. Lannin, Solid State Commun. **40,** 81 (1981).

[43] P. J. Carroll, J. S. Lannin, J. Non-Crystall. Solids **35/36,** 1277 (1980).

[44] T. Mori, S. Onari, T. Arai, J. Appl. Phys. **19,** 1027 (1980).

[45] S. Onari, K. Matsuishi, T. Arai, J. Non-Crystall. Solids **74,** 57 (1985).

[46] J. C. Phillips, J. Non-Crystall. Solids **43,** 37 (1981).

[47] M. F. Thorpe, J. Non-Crystall. Solids **57,** 355 (1983).

[48] K. Tanaka, Phys.Rev. **B 39,** 1270 (1989).

[49] T. Wagner, S. O. Kasap, Phil.Mag. **B 74,** 667 (1996).

[50] Z. Borisova, "Glassy Semiconductors" (Plenum Press, New York, 1981).

[51] P. Boolchand, M. Jin, D. I. Novita, S. Chakravarty, J. Raman Spectroscopy **38,** 660 (2007).

[52] E. Ahn, G. A. Williams, P. C. Taylor, Phys.Rev. **B 74,** 174206 (2006).

[53] K.Tanaka, N. Odajima, Solid State Commun. **43,** 961 (1982).

[54] R. T. Phillips, J. Non-Crystall. Solids **70,** 359 (1985).

[55] Powder Diffraction File (ASTM card), ed. L.G.Berry (Joint Committie on Powder Diffraction Standard, Philadelphia, 1974).

[56] R. Zallen, M. L. Slade, A. T. Ward, Phys. Rev. **B3,** 4257 (1971)

[57] M. Abkowitz, R. C. Enck, Phys. Rev. **B27,** 7402 (1983).

[58] V. I. Mikla, Dr.Sci. Thesis, Institute of Solid State Physics, (Academy of Sciences, Kiev, 1998).

[59] J. C. Phillips, Solid State Phys. **10,** 165 (1982).

[60] V. I. Mikla, D. G. Semak, A. V. Mateleshko, A. A. Baganich, Phys. Stat. Solidi (a) **117,** 241 (1990).

[61] V. K. Malinovsky, V.P.Sokolov, Solid State Commun. **57,** 757 (1986).

[62] A. J. Martin, W.Brenig, Phys. Status Solidi **B 63,** 163 (1974).

[63] R. J. Nemanich, Phys. Rev. **B 16,** 1655 (1977).

[64] H. Kawamura, F. Fukumasu, Y. Hamada, Solid State Commun. **43,** 229 (1982).

[65] G. Lucovsky, F. L. Galeneer, J. Non-Crystall. Solids **35/36,** 1209 (1980).

[66] J. Jakle, in: Amorphous Solids: Low-Temperature Properties, Ed. W.A.Phillips, (Springer-Verlag, Berlin, 1981), p. 135.

[67] V. K. Malinovsky, V. N. Novikov, V. P. Sokolov, Phys. I Khim. Stekla, **15,** 331 (1989).

[68] G. Lucovsky, J. Non-Crystall. Solids **97/98,** 155 (1987).

[69] H. Richter, Z. P. Wang, L. Ley, Solid State Commun. **39,** 625 (1981).

[70] V. A. Bagrynskii, V. K. Malinovsky, V. N. Novikov, L. M. Puschaeva, A. P. Sokolov, Fiz. Tverd. Tela **30,** 2360 (1988).

[*]Corresponding author: victormkl836@gmail.com